BIOCHEMISTRY
including biophysical chemistry & molecular biology
Article

Biochemistry **2010,** *49,* 267–278 267
DOI: 10.1021/bi901634p

Structural Guidance of the Photocycle of Channelrhodopsin-2 by an Interhelical Hydrogen Bond†

Christian Bamann,*,‡ Ronnie Gueta,§ Sonja Kleinlogel,‡ Georg Nagel,§ and Ernst Bamberg‡,∥

‡*Max-Planck-Institut für Biophysik, Max-von-Laue Strasse 3, 60438 Frankfurt, Germany,* §*Universität Würzburg, Botanik I, Julius-von-Sachs-Platz 2, 97082 Würzburg, Germany, and* ∥*Johann Wolfgang Goethe-Universität, Institut für Biophysikalische Chemie, Max-von-Laue-Strasse 9, 60438 Frankfurt, Germany*

Received September 18, 2009; Revised Manuscript Received November 17, 2009

ABSTRACT: Channelrhodopsin-2 (ChR2) is a light-gated cation channel and a member of the family of retinylidene photoreceptors. Since the demonstration of light-induced depolarization of ChR2-expressing animal cell membranes, it was increasingly exploited for light triggering of action potentials. ChR2 conducts cations upon light absorption that embodies retinal isomerization as the primary reaction and a structurally unknown opening mechanism. It is evident from spectroscopic data that protonation reactions at the Schiff base are part of the photocycle, comparable to other microbial-type rhodopsins. However, the connection between the processes at the chromophore site and the channel's pore remained enigmatic. Here, we use slow mutants of ChR2 that we generated by disturbing a postulated hydrogen bond when mutating C128 in the transmembrane (TM) helix 3 and D156 in TM helix 4. The lifetime of the mutants' open state is increased more than 100 times. We investigated the spectral properties of the slow mutants. Whereas the deprotonation of the Schiff base (yielding P390) occurs on the same time scale as that of the wild type, reprotonation to P520 is retarded in the slow mutants and their photocycle is split, leading to the presence of two photointermediates, P390 and P520, in the open state. The photoreactions of P390 and P520 lead to a quenching of the current in electrophysiological measurements. We conclude that the putative hydrogen bond between C128 and D156 is an important structural determinant of the channel's closing reaction. Furthermore, we show that the D156A mutant is even more suitable for light control of excitable cells than C128A.

Channelrhodopsins (ChRs)[1] are light-gated cation channels (*1*, *2*) that belong to the family of retinal photoreceptors. Originally, they operate as part of the photosensoric machinery in the unicellular alga *Chlamydomonas reinhardtii* (*3*). ChR1 can mediate photophobic and phototactic responses under a wide range of conditions, whereas the contribution and function of ChR2 are obscure in the cell (*4*). On the other hand, it is ChR2 that has proven to be an excellent tool for the light activation of neurons, because it induces a much higher conductance.

Heterologous expression of ChRs promotes light sensitivity in the host system. In excitable cells, light activation depolarizes the cell membrane and eventually leads to the firing of action potentials (*5*, *6*). The concept of installing an optical switch can be extended by the chloride pump halorhodopsin that is spectrally shifted compared to ChR2. The outwardly directed chloride pump current hyperpolarizes the cell and leads to the silencing of neurons establishing an optogenetic control for the on and off state of excitable cells (*7*). This application has been documented in numerous publications and systems. Noteworthy is the extension to living complex organisms. The first demonstration was the light-induced muscle contraction in the nematode *Caenorhabditis elegans* (*8*) followed by the expression in rodents (*9*), *Drosophila* (*10*), zebrafish (*11*), or macaque (*12*).

Until now, its advanced practical implementation is in contrast to our molecular understanding of the ChRs. A deeper mechanistic insight will guide the generation of new variants with tuned molecular properties and vice versa like altered absorbance spectra, kinetics, or cation selectivities. Because of the sequence homology of ChR2, bacteriorhodopsin (bR) is used as a blueprint in a structure−function context. Microbial rhodopsins share a common seven-transmembrane helix motif with a retinal chromophore bound to the side chain of a lysine residue, forming a protonated Schiff base. The light reaction isomerizes the retinal moiety around the C13 double bond, initiating an orchestrated sequence of events that leads to vectorial transport of a proton from the cytoplasmic to the extracellular side (*13*). The appearance of different photocycle intermediates can be followed because of their altered spectral properties. Mechanistically important for the proton pumping mechanism proves to be the blue-shifted M state (M_{410}) with a deprotonated Schiff base. De- and reprotonation to different sides are crucial for the vectoriality of the pump. Initial characterization of wild-type ChR2 led to the identification of several spectral intermediates present during its photocycle in a single turnover (*14*, *15*). An early intermediate, P500, is formed in nanoseconds from the ground state, D470, and is converted to a state with a deprotonated Schiff base, P390, in microseconds before the opening of the channel. During its open

†This work was supported by the Deutsche Forschungsgemeinschaft (SFB 807 to E.B. and SFB 487 to G.N.), the Cluster of Excellence Frankfurt Macromolecular Complexes, and the Max-Planck-Society.

*To whom correspondence should be addressed: Max-Planck-Institute of Biophysics, Department of Biophysical Chemistry, Max-von-Laue-Strasse 3, 60438 Frankfurt, Germany. Telephone: ++49-69-6303 2007. Fax: ++49-69-6303 2222. E-mail: Christian.bamann@biophys.mpg.de.

[1]Abbreviations: ChR, channelrhodopsin; bR, bacteriorhodopsin; DM, *n*-decyl *β*-maltoside; HBW, spectral half-bandwidth; PDB, Protein Data Bank.

Published on Web 12/11/2009

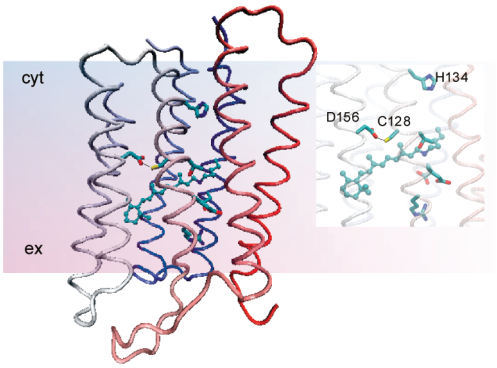

FIGURE 1: Structural model of ChR2. The model [SWISS-MODEL (*52*)] is based on the structure of bR (PDB entry 1C3W) with the indicated orientation toward the cytoplasmic (cyt) and extracellular (ex) side. The hydrogen bond between C128 and D156 is indicated as a dotted line connecting transmembrane helices 3 and 4. The inset shows the environment around the retinal binding pocket with the aforementioned residues and the one contributing to the counterion (T127, E123, D253, and R120, not indicated) and H134, homologous to the proton donor D96 in bR. This figure was produced with VMD (*53*).

lifetime, a third species is present, P520, that decays concomitantly to the closing process of the channel within milliseconds. The ground state is restored in seconds from a spectrally similar species, P480, that is associated with a desensitized state in current measurements (*14*). Recent data from vibrational spectroscopy revealed further characteristics of ChRs: Light leads to major structural perturbations compared to bR that start with the P500 intermediate and persist in the presence of P480 (*15*, *16*). Reisomerization of the retinal seems to be decoupled from the conformational changes and follows the closing of the channel. Despite the similarities to the photocycles of other microbial rhodopsins, the transduction of the light reaction to the pore structure remains enigmatic.

Recently, the slow C128X variants of ChR2 have been used to demonstrate their applicability in neuronal cell cultures (*17*). The potential use of these so-called bistable switches that relies on their long open times was emphasized. Brief blue light pulses depolarize the membrane in a stable manner for several seconds. This can be reverted by red light in milliseconds. Both the on and off kinetics were changed for the channel conductance when the cysteine at position 128 was changed to a threonine, alanine, or serine. The homologous residue in bR is T90 that is hydrogen-bonded to D115 located at the neighboring transmembrane helix 4. Both residues are conserved among many archaebacterial rhodopsins (*18*). T90 is located close to the retinal binding pocket (Figure 1) within 4 Å of the carbon atoms of the methyl groups at C13 (retinal) and the threonine side chain (PDB entry 1C3W) that is hydrogen-bonded to the aspartate side chain of D115 (*19*). Both residues are not part of the proton transfer pathway for the vectorial transport in bR. However, mutations at this position have effects on the phenotype of bR. The isomer composition, the proton transport efficiency, and the photocycle kinetics are affected (*20*, *21*). A deeper investigation of the D115A mutant emphasized the importance of the hydrogen bond between T90 and D115 that coordinates the dynamics in the cytoplasmic proton half-channel and the sequestered reprotonation of the Schiff base by the primary proton donor D96 (*21*).

So far, these slow mutants with their intriguing phenotype have been described only on the basis of electrophysiological measurements. However, no spectral information was given to set a rationale for the altered properties. It is attractive to combine the functional data about the channel's conductivity with spectral data. This approach turned out to be fruitful for the wild type (*14*). To investigate further the importance of the hydrogen bond between C128 and D156, we reinvestigated the electrical data of the C128X mutants and compared them to the D156A construct.

Two main differences from the wild type could be identified in the spectroscopic part: the presence of two long-lasting spectral intermediates, P390 and P520, and the splitting of the photocycle. Both photointermediates could be confirmed in current measurements on oocytes. The photoreaction of P390 has not been described so far for ChR2, and its presence links the P390 intermediate with the open state of the channel beside the before identified P520.

D156A has in current measurements a phenotype similar to that of the C128X mutants. However, we demonstrate a superior applicability in neurons for light-induced depolarization. This is due to the fastest opening kinetics of the channel among all the slow mutants and an open lifetime persisting over minutes. As shown for the C128X mutants (*17*), the channel can be reliably closed by the excitation of the P520 intermediate in the millisecond time domain that is also true for the D156 mutant. The similarity of the slow phenotype emphasizes the functional linkage between helix 3 (C128) and helix 4 (D156) in channelrhodopsins. While they confer a higher light sensitivity to their expressing hosts, they point to a key structural element for the transduction of the light reaction to the channel's functional state.

MATERIALS AND METHODS

Expression and Purification of ChR2 in Pichia pastoris. The cDNA of chop2 (GenBank accession number AF461397) encoding residues 1−315 with a C-terminal nine-His tag sequence was cloned in the pPIC9K vector (Invitrogen) via its EcoRI and NotI sites. C128T, C128A, and D156A mutants were generated with the QuikChange kit (Stratagene). The correctness of all constructs was validated by sequence analysis. The linearized pPIC9K-chop2(1−315)9His vector was transformed into *P. pastoris* strain SMD1163 (*his4, pep4, prB1*) (Invitrogen). Cell cultures and membrane preparation were performed as described previously (*22*) with several modifications. Briefly, the expression of Chop2 was induced in the presence of all-*trans*-retinal by methanol added three times over a period of 30 h. The cells were harvested by centrifugation and resuspended to 30% wet weight in 20 mM sodium phosphate (pH 7.4), 100 mM NaCl, 2 mM EDTA, 1 mM phenylmethanesulfonyl fluoride (PMSF), and 5% (v/v) glycerol. Cell lysis was induced mechanically by glass beads (0.5 mm) in a bead-beater (BioSpec Products). The suspension was centrifugated (15 min at 5000*g*) for clearing from the cell debris, and the membranes were collected after another centrifugation step (1 h at 100000*g*). The membranes were homogenized in 20 mM HEPES-NaOH (pH 7.4), 100 mM NaCl, and 1 mM PMSF and afterward solubilized in 1% (w/v) decyl maltoside (DM) (Glycon Biochemicals) and 2 M urea for 1 h at 4 °C. After centrifugation (100000*g* for 1 h), the supernatant was loaded on a Ni-NTA Sepharose column (GE Healthcare) and eluted with 500 mM imidazole. The protein samples were concentrated in Centrikon YM-10 concentrators (Millipore) and desalted in 20 mM HEPES-NaOH (pH 7.4), 100 mM NaCl, and 0.2% (w/v) DM with a HiTrap column (GE Healthcare).

Flash Photolysis. Time-resolved spectral changes were recorded on a home-built setup. The measuring light from a 75 W XBO lamp was passed through a gated shutter and a small-band interference filter (Schott) before entering the sample. The gated shutter minimizes the illumination period by the measuring light and reduces ground-state excitation before the actinic laser flash. The light was focused on the entrance slit of a monochromator (minichrom, Optometrics), and its intensity was recorded with a photodiode (UV-005, OSI Optoelectronics). The time resolution was limited to 8 μs. The reaction was started by a laser flash from a broadband dye laser (RDP-1, Radiant Dye Laser Accessories) pumped by a XeCl excimer laser (Lambda Physik). Energies for single flashes amounted to 4−6 mJ for either a Coumarin 2 (λ = 456 nm) or a Coumarin 102 (λ = 477 nm) solution. For longer recordings (> 100 ms), we used a double-beam spectrophotometer (U3000, Hitachi) with a light guide coupled to the quartz cuvette. Starting flashes had an energy of 0.5−1 mJ in this case. This led to an increased stability under low-light intensity conditions of the measuring light that was a prerequisite for avoiding actinic effects from the measuring beam during long time measurements (500 s).

The data were acquired on two digital oscilloscopes (Pro 10 and Sigma 30, LDS-Nicolet). The number of data points was reduced on a logarithmic time basis, and absorbance changes were described with a set of exponential functions in a global fitting routine as described previously (*14*).

Expression of Chop2 Variants in Xenopus Oocytes. Point mutations at positions C128 and D156 were inserted via site-directed mutagenesis (QuikChange kit, Stratagene) into a C-terminally truncated Chop2 variant, encoding amino acids 1−315 in pGEM-HE (*2*). After sequence verification, oocytes from *Xenopus laevis* were injected with 20−30 ng of in vitro-transcribed cRNA (Ambion) and incubated in all-*trans*-retinal (10 μM, from a 10 mM stock in ethanol) containing oocyte Ringer's solution for 2−5 days. Oocytes were tested for light-induced cation conductance by using two-electrode voltage-clamp techniques.

Electrophysiology. In two-electrode voltage-clamp experiments, Chop2 variants C128A, C128T, and D156A were activated and inhibited in the absence of daylight with diode-pumped solid-state (DPSS) lasers with 473 nm (10 mW/mm^2), 405 nm (6 mW/mm^2), and 532 nm (12 mW/mm^2) wavelengths. Measurements were taken in oocyte Ringer's solution in which $CaCl_2$ was substituted with 2 mM $BaCl_2$. Data acquisition was performed using a NI USB-6221 BNC device (National Instruments). Currents were recorded with a Turbo Tec-05X amplifier (NPI Electronic, Tamm, Germany) and the WINEDR program module of Strathclyde Electrophysiology Software (University of Strathclyde, Glasgow, Scotland).

Whole-Cell Patch-Clamp Recordings in HEK Cells. We introduced mutations into the pcDNA3.1-ChR2(1−315) (*2*) plasmid using site-directed mutagenesis (QuickChange kit, Stratagene). The C-terminally truncated version of wild-type ChR2 (encoding amino acids 1−315) is fused in frame with the coding sequence of YFP. HEK293 cells were transiently transfected with cDNAs encoding ChR2(1−315)-C128T, -C128A, -C128S, and -D156A using the effectene transfection kit (QIAGEN, Hilden, Germany). all-*trans*-Retinal (1 μM) was added to the culture medium, and electrophysiological recordings were taken 18−48 h after transfection. Signals were amplified using an Axopatch 200A amplifier (Axon Instruments, Union City, CA), filtered at 2 kHz, digitized with an Axon Digidata 1600 at 5 kHz, and acquired and analyzed using pClamp9 software (Axon Instruments). Patch pipettes with resistances of 2−4 MΩ were fabricated from thin-walled borosilicate glass (GB150-8P, Science Products, Hofheim, Germany) on a horizontal DMZ-Universal puller (serial no. 5318904120B, Zeitz-Instruments, Augsburg, Germany). The pipet solution contained 123 mM cesium gluconate, 7 mM CsCl, 1 mM $MgCl_2$, 5 mM ATP_{Na2}, 10 mM EGTA, and 10 mM HEPES (pH 7.4) (CsOH). The bath solution consisted of 135 mM NaCl, 4 mM CsCl, 1 mM $MgCl_2$, 2 mM $CaCl_2$, 10 mM glucose, and 10 mM HEPES (pH 7.4) (NaOH). Recordings were conducted on an inverted Zeiss Axiovert 25 microscope. The mutants of ChR2 were activated by light pulses from three diode-pumped solid-state lasers (Pusch Opto Tech GmbH; λ_1 = 473 nm, λ_2 = 532 nm, and λ_3 = 593.5 nm), all of which were coupled to a 400 μm optic fiber. Light intensities ranged typically from 20 to 30 mW/mm^2 (details given in figures). Light pulses were applied by a fast computer-controlled shutter (Uniblitz LS6ZM2, Vincent Associates).

Hippocampal Neuron Culture. Hippocampi were isolated from embryonic E18 Sprague-Dawley rats (Jackson Laboratory) and treated with papain (20 units/mL) for 20 min at 37 °C. The hippocampi were washed with DMEM (Invitrogen/Gibco, high glucose) supplemented with 10% fetal bovine serum and triturated in a small volume of this solution with a 1 mL Eppendorf pipet; ~60000 cells in 750 μL of medium were plated on poly-D-lysine/laminin-coated glass coverslips in 24-well plates. After 3 h, we replaced the medium with culture medium (Neurobasal containing 2% B-27 supplement, 2 mM L-glutamine, 100 units/mL penicillin, and 100 μg/mL streptomycin). No all-*trans*-retinal was added to the culture medium or recording medium for any of the experiments described here.

Hippocampal Neuron Electrophysiology. For whole-cell recording in cultured hippocampal neurons, the intracellular solution contained 3 mM NaCl, 10 mM Hepes, 10 mM EGTA, 110 mM D-gluconic acid, 1 mM $CaCl_2$, 1 mM $MgCl_2$, 1 mM ATP_{Na2}, 1 mM ATP_{Mg}, and 1 mM GTP_{Na} titrated to pH 7.3 (KOH). Tyrode's solution was employed as the extracellular solution [125 mM NaCl, 2 mM KCl, 2 mM $CaCl_2$, 1 mM $MgCl_2$, 30 mM glucose, and 25 mM HEPES (titrated to pH 7.4)]. Borosilicate glass pipet resistances ranged from 4 to 8 MΩ. Access resistance was 10−40 MΩ and was monitored for stability throughout the experiment.

RESULTS

Ground-State Spectra. The D156A and C128X variants and the wild type were transformed in the yeast *P. pastoris* and purified from the membrane fraction as described for the fusion protein between the wild type and the yellow fluorescent protein (*14*). In Figure 2, the spectra for the ground states are compared. The wild type exhibits two peaks at 447 and 470 nm with a shoulder at 410 nm. The vibronic fine structure is in agreement with the published data for ChR2 from *Chlamydomonas reinhardtii* (*14*, *15*) and the VChR1−VChR2 chimera (*23*). A similar appearance was observed before for the sensory rhodopsins II (*24*, *25*). The spectra of the C128T and D156A mutants are red-shifted with a dominant peak at 480 nm and two minor ones at 450 and 415 nm. In contrast to the two former variants, expression of a functional C128A holoenzyme turned out to be more difficult. This variant is prone to aggregation, and the apoenzyme does not reconstitute efficiently with all-*trans*-retinal as judged from the baseline scattering and the 280 nm to

470 nm absorbance ratio. In addition, minor peaks around 350 nm can be observed for the C128X mutants that are most likely species with a deprotonated Schiff base. Their population is higher in the C128A and D156A mutants.

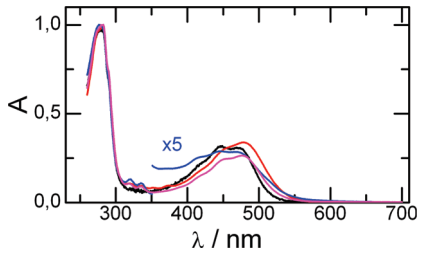

FIGURE 2: Ground-state spectra of ChR2. Ground-state spectra are normalized to the absorbance at 280 nm recorded in 20 mM HEPES (pH 7.4), 100 mM NaCl, and 0,2% DM. The spectrum of C128A is scaled in the visible part of the spectrum for the sake of comparison. The wild-type spectrum is colored black, the C128T spectrum red, the C128A spectrum blue, and the D156A spectrum pink.

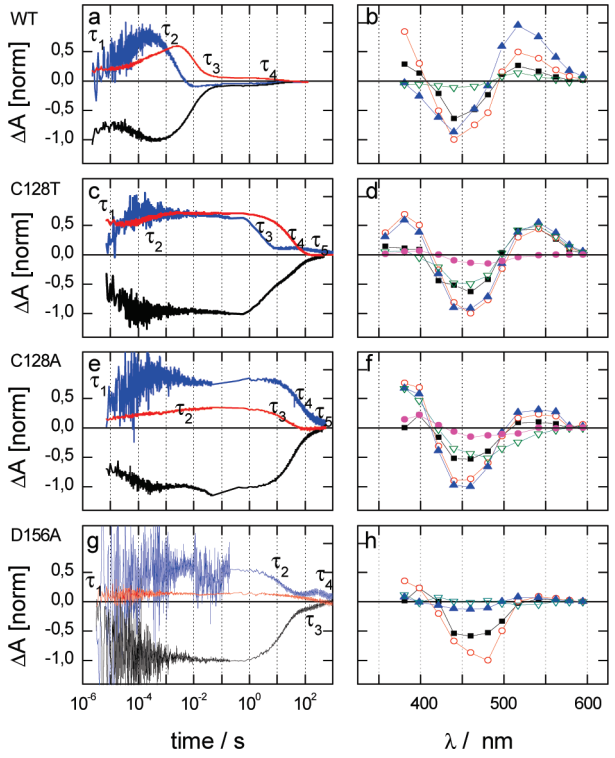

FIGURE 3: Transient absorbance changes of ChR2 mutants compared to the wild type. Time courses of absorbance changes for the wild type (a) and the C128T (c), C128A (e), and D156A (g) mutants, followed at three characteristic wavelengths, representing the ground state D470 (black line), the P390 intermediate (blue line), and the P520 intermediate (red line). The time constants from a global fit analysis are included to indicate the intermediates' transitions (see the text). From a linear photocycle model, we extracted the spectral intermediates that correspond to the time constants that are represented for the three variants in panels b, d, f, and h: (■) P_1 (black), (○) P_2 (red), (▲) P_3 (blue), (▽) P_4 (green), and (●) P_5 (pink).

Flash Photolysis. We followed the absorbance changes after a flash excitation at 450 or 480 nm. Spectral shifts were observed in a time interval ranging from microseconds to hundreds of seconds. In Figure 3a,c,e,g, the characteristic wavelengths of the spectral intermediates are depicted, i.e., the blue-shifted intermediate P390, the red-shifted intermediate P520, and the ground state D470. It compares the detected time course of the absorbance signals between the wild type and the C128T, C128A, or D156A mutant. For the sake of consistency, we denote the spectral intermediates of the mutants in the same manner as for the wild type and in a manner similar to that of Ritter et al. (*15*).

It is obvious that we observe similar photointermediates in all three variants of channelrhodopsin 2. However, the lifetimes and the decay-associated spectra are different. To describe the time course of the absorbance signal of the slow mutants, we need four and five relaxation time constants as determined from a global fit analysis that are summarized in Table 1. After light excitation, a red-shifted intermediate appears that is beyond the time resolution of our system and therefore present as an offset in the 541 nm signal. This early intermediate indicates a protonated Schiff base and has been identified before as the P500 species resembling the K state of bR (*15*). In a subsequent process, the Schiff base is deprotonated in the microsecond time region, while the P500 intermediate decays as observed on the decreasing amplitude of the 541 nm signal (τ_1 in Figure 3c). The kinetics of P390 formation is comparable in all four variants of ChR2, and slightly faster in the C128X mutants. In the next step, we observe the rise of the P520 intermediate where we can detect differences between the wild type and the mutants. In the wild type, the P390 intermediate turns into P520 (τ_2 in Figure 3a), whereas in the C128X and D156A mutants, we observe concurrently the P390 and P520 species. There is a slight spectral shift, when P390 equilibrates with P520. Despite the small amplitude, the process can be clearly followed in the trace at 541 nm denoted with τ_2 (Figure 3c,e). After 10 ms, both of the photointermediates are present in the C128T, C128A, and D156A mutants without any further change for the next 3 orders of magnitude in time. Slight changes in the absorbance traces for the C128A mutant are the result of an actinic effect from the measuring light.

As previously noted, we detect the relaxation of the P520 intermediate in the wild type (τ_3 in Figure 3a) followed by the conversion from the light-adapted, P480, form to the ground state, D470, in seconds (τ_4 in Figure 3a) (*14*). At this stage, we notice the second fundamental difference in the spectroscopic signals from the slow mutants. While both photointermediates persist over several seconds, they decay in two separate relaxation processes with the P390 intermediate as the faster one followed by P520 for the C128T and D156A mutants or vice versa for the C128A mutant (τ_3 and τ_4 in Figure 3c,e and τ_2 and τ_3 in Figure 3g). In the C128T mutant, the P390 intermediate relaxes

Table 1: Relaxation Time Constants from Global Fit Analysis of the Flash Photolysis Data[a]

	P500 → P390	P390 → P520	P390 → D470	P520 → P480	P480 → D470
wild type	τ_1 = 58 μs (5)	τ_2 = 1.8 ms (0.1)	–	τ_3 = 8.5 ms (1)	τ_4 = 10 s (1)
C128T	τ_1 = 33 μs (5)	τ_2 = 0.33 ms (0.043)	τ_3 = 2.2 s (0.1)	τ_4 = 29 s (2.2)	τ_5 = 510 s (155)
C128A	τ_1 = 47 μs (15)	τ_2 = 3.7 ms (1.8)	τ_4 = 42 s (1.4)	τ_3 = 30 s (1.3)	τ_5 = 650 s (182)
D156A	τ_1 = 87 μs (6)	–	τ_2 = 17 s (0.1)	τ_3 = 300 s (4)	τ_4 = 800 s (120)

[a]Values were derived from a global fit. Standard errors are given in parentheses. The relaxation time constants are denoted in the same manner as in Figure 3.

back to the ground state with a time constant τ_3 of 2.7 s, followed by the P520 intermediate ($\tau_4 = 35$ s). Both of these processes are reflected in the time course of the light-adapted state P480. Subtle spectral changes, blue-shifted to the ground state, persist over hundreds of seconds before relaxing back to the ground state ($\tau_5 = 435$ s). For C128A, the separation of the two processes is not as distinct as in the C128T mutant. First, the P520 intermediate relaxes ($\tau_3 = 31$ s) followed by the P390 decay ($\tau_4 = 41$ s). The blue-shifted light-adapted form converts to the ground state in a similar slow process as for the C128T mutant ($\tau_5 = 463$ s). The quality of the D156A traces is limited with respect to the signal-to-noise ratio in the fast time regime, because the data are recorded without averaging. Therefore, it is difficult to follow the equilibration between P390 and P520 as in the other mutants, i.e., τ_2 for C128X. Still, it represents the mutant with the slowest kinetics, retaining comparable spectral characteristics. First, we observe the decay of P390 ($\tau_2 = 17$ s), followed by the P520 intermediate ($\tau_3 = 303$ s) and an additional even slower process ($\tau_4 = 800$ s).

The spectral properties of the kinetic intermediates are summarized in Figure 3b,d,f,h as they are derived from a linear photocycle. Both photointermediates are clearly visible with peaks at around 520 and 390 nm, whereas P520 is slightly red-shifted in the mutants compared to the wild type. This seems to be also true for the early intermediate that has the same spectral characteristics as the late red-shifted photointermediate, although the time resolution and the signal-to-noise ratio especially for the C128A mutant and the D156A mutant add a higher degree of uncertainty for the first photointermediate. However, we denote it as P500 for the sake of comparison. While we observed in the wild type predominantly the P520 intermediate during the open state of the channel (*14*) and the channel closes concurrently with the relaxation of the P520 intermediate, both spectral species, the P390 intermediate and the P520 intermediate, are present during the open state of the C128X and D156A mutants. Furthermore, the ground state is repopulated from both intermediates. Summarizing the comparison with the wild type, we conclude that the processes up to the deprotonation of the Schiff base are similar. Afterward, two crucial differences take place: the spectral intermediates last 3 orders of magnitude longer in the mutant, and the subsequent relaxation of the P390 and P520 intermediates to the ground state does not follow a simple linear scheme of intermediates as in the wild type.

Influence of pH and Light on the Spectral Properties. Several models could account for the time course of the mutants' spectral changes, i.e., branching of the photocycle or a heterogeneous ground state leading to two photocycles. Therefore, we varied our experimental conditions to separate the two rationales. In most cases, we concentrated on the C128T mutant for the spectral studies.

A mixture of two or more spectrally similar states could result in the presence of the three peaks in the ground-state spectra besides a possible vibrational fine structure as mentioned above. However, excitation at different wavelengths (439, 456, or 477 nm) did not change the amplitude ratio of the two different photointermediates, P390 and P520. Therefore, the possibility of two photocycles from two spectrally different states can be ruled out.

As a next parameter, we varied the pH of the solution and looked at the ground-state spectra and at the time-resolved ones. Two pH-dependent ground states have been identified in the visible spectrum for the VChR2−VChR1 chimera (*23*) and for

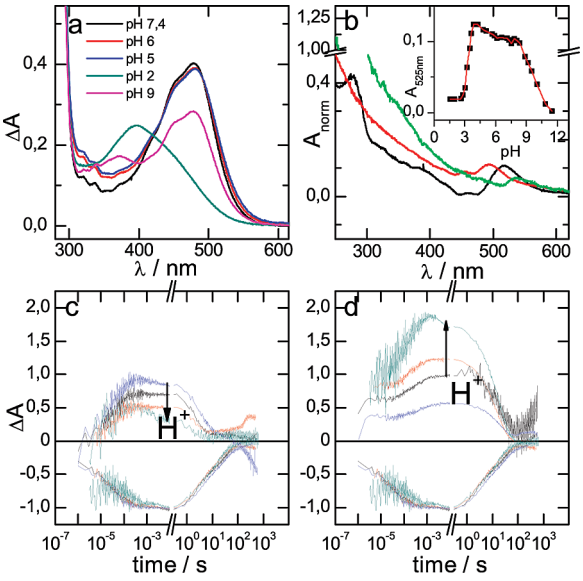

FIGURE 4: Proton-dependent effects on the C128T mutant. (a) Ground-state spectra at different pH values. (b) Difference spectra for pH 5 to the ground state at pH 7.4. The black trace depicts the C128T spectrum, the red one the wild-type spectrum, and the green one the C128A spectrum. For the sake of comparison, the spectra at pH 7.4 were normalized to the 480 nm absorption. The inset shows the titration curve for the C128T mutant followed at 525 nm. (c and d) Spectral changes after flash excitation at four different pH values (green trace for pH 4, red trace for pH 6, black trace for pH 7.4, and blue trace for pH 9) for the C128T mutant for the P390 intermediate (c) and the P520 intermediate (d) in comparison to the ground state (439 nm) in the negative part of the *y*-axis. The signals are normalized to the maximal difference at 439 nm. The onset of the 381 nm trace at pH 4 is digitally filtered at 20 kHz for the sake of clarity.

ChR1 (*4*). The glutamic acid E87 in helix 1 of ChR1 has been identified (*26*) as the protonation site. This residue is not conserved among ChRs (presumably A48 for ChR2). For the C128T mutant, we observe a small change in its absorbance spectrum (Figure 4a) with a decrease in pH from 7.4 to 5. A further decrease leads to an irreversible change and a pronounced hypsochromic shift. A similar behavior is observed on the alkaline branch of the titration curve. The spectrum at pH 9 shows the onset of the hydrolysis of the retinal as indicated by the peak at 375 nm.

Compared to the changes at extreme pH values, the amplitude of the bathochromic shift is minor in the pH range between 8 and 5 (inset of Figure 4b). However, a noticeable red shift can be clearly traced to a form losing the fine structure when the pH is lowered. It is not a special property of the mutant; its presence is detected in the wild type and the C128A mutant (Figure 4b). Similar processes have been reported for other microbial rhodopsins (*27*−*29*), and they have been associated with the titration of the proton acceptor site. However, the spectral changes are more pronounced in these cases. For ChR2, we cannot follow in full the titration due to the acidic denaturation at low pH values.

In complementary experiments, we investigated the influence of the proton concentration on the photocycle of C128T. Three characteristic wavelengths are depicted in panels c zand d of Figure 4, i.e., 439 nm as a measure for the ground state D470, 381 nm for the blue-shifted intermediate P390, and 542 nm for the red-shifted P520. The kinetics are almost not affected by a change in pH to 9 or 4 that can be best followed by the 439 nm traces. The decay of P520 is influenced the most, leading to an approximately

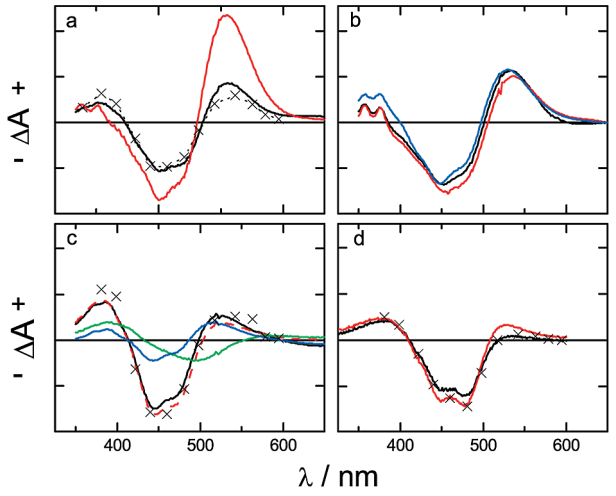

FIGURE 5: Comparison of the C128T and C128A mutants of the photostationary state and kinetic intermediate P3. (a) Photostationary difference spectra after illumination for 3 s (black line) and 30 s (red line) with light from a 75 W XBO passed through a broadband interference filter (HBW of ca. 50 nm) centered at 450 nm (K45). The crosses mark kinetic intermediate P3 from the single-turnover measurements with the spectral intermediates P390 and P520 present. (b) Photostationary difference spectra of the C128T mutant at different pH values (black for pH 7.4, red for pH 6, and blue for pH 9). (c) Photostationary difference spectra of the C128A mutant after illumination for 30 s (black) and 90 s (red) with the K45 filter (λ_{max} = 450 nm) or after 30 s with a K40 filter (λ_{max} = 400 nm; blue line) or a K55 filter (λ_{max} = 550 nm; green line). The crosses indicate kinetic intermediate P3 from the single-turnover measurements. (d) Photostationary difference spectra of the D156A mutant after illumination for 3 s (black) and 30 s (red) with the K45 filter (λ_{max} = 450 nm). The crosses indicate kinetic intermediate P2 from the single-turnover measurements.

2-fold faster time course at pH 4. However, the amplitude ratio of the photointermediates is affected: a higher pH favors the buildup of P390, while a larger amount of P520 is observed at lower pH values. This results from two different processes. First, the offset in the 542 nm trace (Figure 4d) rises with a decrease in pH, and second, the transition from P390 and P520 (τ_2 in Figure 3c) is faster, shifting the equilibration toward P520.

These results indicate the presence of two forms in different protonation states. The spectral shift of the chromophore indicates a change in the electrostatic environment of the protonated Schiff base. Usually, this phenomenon is attributed to the protonation of the counterion, e.g., D85 for bR (*30*) or D97 for protheorhodopsin (*28*). The latter represents an example for an aspartate with a pK_a of 7.7 in the range of physiological pH. At this stage, we cannot conclusively identify the protonation group in ChR2. The minor spectral changes of the ChR2 ground states argue for a distant proton binding site that is not directly linked to the chromophore. However, the effect on the photocycle and its intermediates is evident.

In a next step, we looked into the influence of light on the presence of the photointermediates. Continuous illumination was achieved with light from a XBO lamp passing broadband interference filters (spectral half-bandwidth, HBW, of ca. 50 nm). Using the K45 filter (maximal transmission λ_{max} = 450 nm) generates the photostationary state (Figure 5). This is fairly represented for the C128A or D156A mutant by the kinetic difference spectrum of P3 or P2, respectively, from the linear photocycle resembling the two spectral intermediates P390 and P520 (Figure 5c,d). However, there is a marked difference for the C128T mutant in the spectra of the photostationary state that evolves upon prolonged illumination (Figure 5a). After illumination for 3 s, the spectral changes are in good agreement with the data from the single-turnover measurements. Longer periods of light lead to a bathochromic shift of the P390 intermediate, and furthermore, distinct peaks at 357 and 376 nm that are reminiscent of the fine structure of the ground state evolve. These changes remain in the dark before relaxing in hundreds of seconds and might be caused by the generation of other isomers. The presence of this shift is at least in the photostationary measurements dependent on the mutation of the C128 residue. In the case of the C128A mutant or the wild type, such a phenomenon is not seen. However, similar peaks are observed in the ground state of the C128A and D156A mutants (Figure 2).

The proton concentration does not manipulate the amplitude ratio of the photointermediates of the C128T construct in the same manner as in the single-turnover measurements, always favoring the accumulation of P520 at the measured pH values (Figure 5b). Most of the molecules will be trapped in the long-living P520 state reflecting the much slower relaxation of P520 compared to P390 (see Table 1) that holds under all conditions.

As a last determinant, we investigated the photoreactions of the photointermediates themselves under stationary conditions by changing the excitation wavelength using filters that either excite the D470 and P390 (λ_{max} = 400 nm; K40 filter) or D470 and P520 (λ_{max} = 550 nm; K55 filter) states. This is exemplified for the C128A mutant (Figure 5c). Indeed, the different amplitude ratios point to additional photoreactions in the photocycle. Green light (K55) shortens the lifetime of P520 and results in a relatively higher level of accumulation of P390. This green light effect has been shown before for the wild type (*14*) and the C128X mutants (*17*). The effect of violet light (K40) can accordingly be explained by the photoreaction of P390 back to the ground state. Here, we observe a larger amount of P520. The light reaction of P390, similar to the blue light effect in bR (*31*), has so far not been described for ChRs.

Kinetics of Conductance Changes. In electrophysiological experiments, we extended our spectral investigation to the C128S and D156A mutants in addition to the C128T and C128A mutants. The C128X variants were initially investigated before (*17*) but so far not related to the spectral analysis. Here, they represent a benchmark for the D156A mutant. Furthermore, the functional interaction between the two residues has not been shown.

We could express the D156A and C128X mutants in cells of different origins for their functional characterization. Despite their pronounced difference in the photocycle kinetics, all of the C128X variants are functional as light-gated cation channels (*17*). Upon illumination, the channel opens with a retarded kinetic compared to the wild type in all four forms (see Table 2 and Figure 6a). The process is moderately accelerated with an increase in the external proton concentration pH_o, e.g., from 5 ms at pH_o 7.6 to 2.5 ms at pH_o 4 for the C128T mutant. The opening of the channel is not clearly accompanied in a parallel process at the chromophore site. This is true at least for the C128T mutant where the opening proceeds in the early millisecond time domain with no spectral counterpart. The slow opening is observed under single-turnover conditions, too (data not shown), i.e., strictly comparable to the spectroscopic measurements. Hence, it is a result of the intrinsic kinetic behavior of the enzyme.

Whereas the wild type is desensitized in milliseconds, we do not observe such a pronounced effect of the steady-state current at

Table 2: Relaxation Time Constants from the Electrophysiological Data[a]

	τ_{on} (ms)	τ_{off} (ms) (dark)	τ_{off} (ms) (405 nm)	τ_{off} (ms) (532 nm)	τ_{off} (ms) (593 nm)	$J_{0.5}$ (mW/mm^2)
wild type[b]	0.2	10	–	–	–	0.7
C128T	5.7 (1.4)	1.7×10^3 (10^2)	21 (3)	8.8 (0.6)	–	0.03
	[9.0 (1.6)]	[2450 (500)]		[8.7 (1.9)]	[340 (170)]	
C128A	7.9 (3.1)	3.9×10^4 (1.3×10^4)	29 (5.2)	9.6 (1.7)	–	0.01
	[5.7 (1.0)]	[4.9×10^4 (1.8×10^4)]		[28 (1.0)]	[250 (20)]	
C128S	13 (1.7)	2.8×10^4 (8.1×10^3)	–			0.01
	[30 (7.5)]	[1.0×10^5 (1.1×10^4)]		[4.2 (1.2)]	[32 (6.3)]	
D156A	5.0 (0.7)	$>1.5 \times 10^5$[c]	–			0.01
	[3.3 (0.1)]	[3.2×10^4 (2.5×10^3), $>1.5 \times 10^5$[c]]		[13 (0.6)]	[480 (22)]	

[a]The top row of data for each mutant corresponds to the oocyte measurements, while the bottom row was taken from the HEK cell measurements. These values are in brackets. The τ_{off} values with different background light are measured with 100% light intensity as indicated in Figures 5 and 6. Apparent half-saturating light intensities ($J_{0.5}$) are taken from the stationary currents in oocyte measurements with blue light excitation (473 nm; 1 mW/mm^2 = 2.4×10^{17} cm^{-2} s^{-1}). The standard errors are given in parentheses. [b]The wild-type data besides the $J_{0.5}$ value were taken from ref *2*. [c]The data cannot be determined accurately and represent a lower limit estimation. In the HEK cell measurements, the two phases account for approximately 50%.

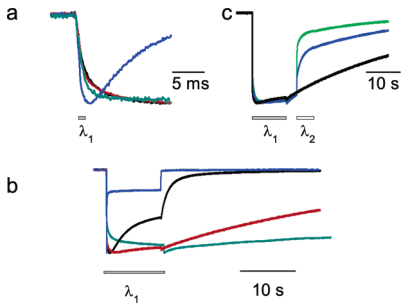

FIGURE 6: Light activation of Chop2 mutants in oocytes from *X. laevis*. Photocurrents were recorded with a two-electrode voltage clamp in Ringer's solution at a holding potential of −100 mV. Overlay of normalized photocurrents of oocytes expressing the wild type (blue), C128T (black), C128A (red), or D156A (cyan) after a 1 ms laser flash (a) (λ_1 = 473 nm; 10 mW/mm^2) and or a 10 s laser flash (b). (c) Rapid closing and inhibition of C128A after activation for 10 s with 473 nm (λ_1) when stimulating for 5 s with a λ_2 of 532 nm (green line) and a λ_2 of 405 nm (blue trace) or in the dark (black line). Currents are typical of those in five other experiments.

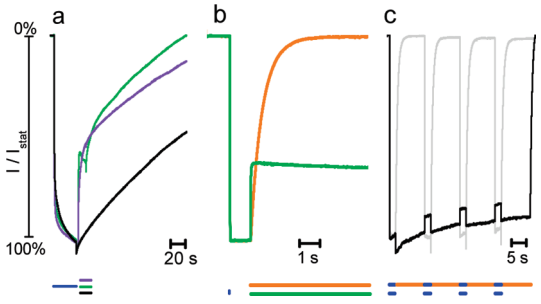

FIGURE 7: Photocurrents of *X. laevis* oocytes and HEK293 cells expressing D156A. (a) Inhibition of D156A after a 40 s 473 nm laser application with a 10 s 532 nm (green) and 405 nm laser application (violet) in oocytes. Photocurrents without inhibition are colored black. (b) Photocurrents and accelerated closing by light stimulation in HEK293 cells. Photocurrents were triggered by a 20 ms blue light pulse (473 nm) at −60 mV. Off kinetics were accelerated with a second light pulse of orange light (593.5 nm, orange trace) or green light (532 nm, green trace). All light intensities were adjusted to 26.9 mW/mm^2. (c) Control of on and off states with blue and orange light. The gray trace is the result of the alternating illumination pattern as indicated at the top (blue, 473 nm for 20 ms; orange, 593.5 nm for 8 s). The black trace shows the current with a dark period between the blue light stimuli. All photocurrents are normalized to the stationary current.

longer illumination times (Figure 6b). The desensitization process as observed in the transition from a peak to the stationary current can be observed best in the C128T mutant and worst in the D156A mutant. The effect is correlated with the closing time constant and hence with the open probability. A small increase in the stationary current is observed when the light is switched off. Therefore, a larger number of open channels are accumulated transiently (see below), which has also been observed by Berndt et al. (*17*).

The slow relaxation of the photointermediates is reflected in the closing time of the channel, too, ranging from 1.7 s for the C128T mutant to 40 and 30 s for the C128A and C128S variants, respectively. The D156A mutant closes in two phases, whereas the first one is similar to the C128A mutant (τ_{off} = 30 s), accounting for ~50% of the total amplitude in the HEK cell measurements. In oocytes, the closing event is even slower (Figure 7a). We could not accurately determine the complete return to the closed state in voltage-clamp experiments because of the long settling time. The complete return to the closed state cannot be estimated following current relaxation for 5 min in the dark; i.e., the τ_{off} exceeds 10 min. In contrast to that of the wild type, the closing reaction is not affected by the membrane potential. Lowering the pH_o leads to a faster current decay in the slow mutant forms, e.g., from 20 s at pH_o 7.6 to 10 s at pH_o 4 for the C128A mutant.

The longer lifetime of the open state is reflected in a higher light sensitivity (*17*). The apparent half-saturating light intensities ($J_{0.5}$) are summarized in Table 2. Corresponding to the lifetimes, they are 25 (C128T) to 70 (D156A) times lower than for the wild type. One has to note that the $J_{0.5}$ values are determined by the cycling time and do not report different quantum efficiencies. Ths same kinetic effect has been observed, for example, for the bR D96N mutant that is trapped in the M state (*32*). The apparent $J_{0.5}$ values are smaller than the one determined by Berndt et al. (*17*). So far, we do not have a clear explanation for the discrepancy that can also be observed for the absolute values of $J_{0.5}$; e.g., for the wild type, one can estimate a $J_{0.5}$ value of 5×10^{15} photons cm^{-2} s^{-1} from Figure 1 of ref *17* whereas we determined a value of 1.7×10^{17} photons cm^{-2} s^{-1}, which is closer to the reported value for ChR2 published previously (*9*).

Photocurrents of the Intermediates. The presence of both photointermediates, P390 and P520, can be probed in double-illumination experiments in which the intermediates can undergo photoreactions themselves, which has been shown for P520 in wild-type ChR2 (*14*). Green light (532 nm) leads to a faster closing of the channel (Figure 6c), before the current settles to a

stationary value that is explained by a residual photoactivation of the ground state by green light, which has also been suggested by Berndt et al. (*17*). Shifting the wavelength to even longer values increases the fraction of closed channels at the expense of the closing acceleration (see Table 2); e.g., for the C128A mutant, we still observe a 200-fold faster decay of the current to the baseline under red light illumination (593 nm, 10 mW/mm^2) compared to the dark reaction. This opens up a way for the dichromatic control of the open and closed state of the channel (*17*). The application of different wavelengths with variable intensities tunes the reactivity, i.e., the current amplitude, and the temporal resolution, i.e., the closing rate.

Besides the known green light effect, we could detect in addition a quenching of the stationary current by violet light [405 nm (Figure 6c)]. This light reaction has not been detected before in the wild type. The P390 intermediate is part of the functional cycle of the C128X mutants and reminiscent of the blue light effect of bR (*33*). Hence, both spectral intermediates, P520 and P390, are involved in processes leading to the opening or the closing of the pore. In the C128X mutants, the blue light effect depends on the proton concentration. At pH_o 4, no quenching of the stationary current is observed anymore, where the concentration of P390 is too low to accelerate the closing reaction.

Interestingly, the D156A mutant exhibits the same behavior. Channel closing is affected by either green (532 nm) or violet (405 nm) light (Figure 7a). The phenotype resembles that of the C128X mutants, i.e., a long lifetime of the open state and the quenching sensitivity for the P390 and P520 intermediates. Furthermore, it constitutes the variant with the slowest closing and fastest opening reaction (Table 2). These properties make it even more applicable as a step-up mutant than the C128X mutants. In a first attempt, we looked at the channel characteristics in HEK293 cells. Short light pulses trigger inward currents that remain almost constant for tens of seconds (Figure 7b). Orange or green light accelerates closing. The residual current after closing with longer wavelengths results from ground-state activation. Remarkably, as opposed to the C128X mutants, orange light closes D156A completely within milliseconds. The concept of switching the channel on and off is demonstrated in Figure 7c. Brief pulses of blue light open all channel molecules that remain open for minutes. A second blue light pulse after a dark period even quenches the current. In comparison, orange light reliably switches off the current.

Application in Excitable Cells. The remote light-induced control of excitable cells is the major technological aspect of channelrhodopsins. For comparison to the D156A mutant, we also investigated the C128X mutants, and their usability was contrasted to that of the D156A mutant by expressing the various constructs in hippocampal neurons. All four variants express well in excitable cells, and increased currents compared to wild-type ChR2 can be evoked by blue light (473 nm). Here we focus on the so far not described D156 mutant. The seconds lasting open times enable control of the cells by short (4−10 ms) illumination periods leading to spike trains in current-clamp mode (Figure 8a). Illumination with orange light (593.5 nm) closed the channel within milliseconds. Illumination with green light (532 nm) could be used to switch off firing but to keep the cell in a subthreshold depolarized state. In our hands, no electrical stimulation was needed to reach the firing threshold. The presence of the photointermediates and their effect on the channel closing kinetics can be exploited in achieving suitability for a given

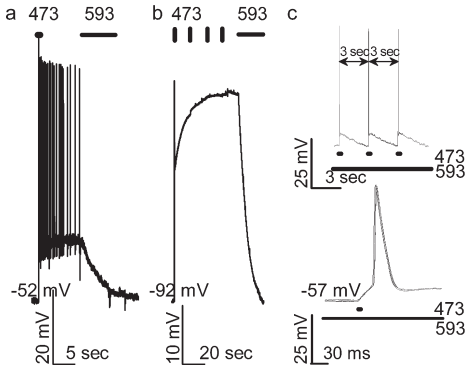

FIGURE 8: Light-induced activation of hippocampal neurons by D156A. (a) Blue light (473 nm, 22.9 mW/mm^2) for 10 ms triggers the firing of action potentials over tens of seconds. Orange light (593.5 nm, 22.9 mW/mm^2) repolarizes the cell and inhibits spiking. (b) Whole-cell current clamp recording. Subthreshold long-term depolarization was induced by a single 10 ms pulse of 473 nm light from a holding potential of −92 mV. Additional blue light pulses every 20 s did not markedly increase the depolarization level. (c) Double illumination with orange background light and blue 4 ms light pulses elicited single action potentials (top). Accurate temporal resolution is shown by an overlay of four sweeps.

experiment. One can either make use of the long open times of the mutants which render increased sensitivity and short stimulation times or achieve high temporal resolution in activity by using two (or three) wavelengths. This is illustrated in Figure 8b,c for the D156A mutant. A short light pulse leads to depolarization of the neuron for minutes (Figure 8b). Background illumination with orange light sufficed to restore the temporal resolution of the wild type, so that short blue light pulses reliably evoked single action potentials (Figure 8c). We emphasize the superiority of the D156A mutant over the C128X mutants for the different neurobiological applications.

DISCUSSION

Suitability of D156A in Neurobiological Applications. Channelrhodopsins proved to be very useful in the optogenetic control of excitable cells (*5*, *7*). Their versatile usage as a tool to light-manipulate membrane potential has been demonstrated from cell cultures to living animals. However, special properties of these molecules are often needed for a particular case, i.e., ion selectivity or spectral shifts of the retinal proteins for their application in imaging techniques. Therefore, one of the major goals is to develop a toolbox with defined molecular properties. So far, the main limitation arises from the maximal light-induced current available. Several factors and characteristics of the channel contribute to the impediment, i.e., the expression level of the channel, its low single-channel conductance (*2*, *34*, *35*), and the open probability that reflects the light sensitivity of the system. C128X and D156A are affected at least in the latter property, showing unusual long open times that are 100−1000-fold longer than for the wild type, leading to an increased sensitivity (*17*). The high temporal resolution of the wild type to trigger single spikes can be re-established simply by the combination of blue light pulses with a background of orange light. The mutants' value is further corroborated in the double-illumination experiments. Single flashes lead to depolarization, with a duration of seconds, that evokes a train of action potentials in single neurons. The duration may be simply tuned by the kind of mutant or even more conveniently by green or red light that shuts off the channel in milliseconds. The mutants'

characteristics combine the special advantages of the optogenetic channelrhodopsin system, i.e., stable and targeted expression controlled on the genetic level and high spatial and temporal resolution controlled on the illumination protocol. The new dichromatic way to modulate the functional state of the channel has been applied in the chemically modified channel systems previously (*36*) that rely on the photoreaction of chemically modified compounds, e.g., azobenzenes or spyropyrans/merocyanines. However, channelrhodopsins are more suited for in vivo application because light sensitivity relies only on the naturally occurring retinal.

Effect of Mutations on the Photocycle. Besides the technical impact of the mutants, their phenotype draws the attention to its biophysical basis. Here, we extended our initial characterization of ChR2 with spectroscopic and electrophysiological methods (*14*). Foremost, this led to the identification of the photoreaction of the P390 intermediate. This result was unprecedented and emphasizes the intermediate's presence in the functional cycle of the channel.

There is an influence on the ground-state spectrum due to the mutations at positions C128 and D156. The minor peaks in the UV region could indicate a subtle change in the retinal binding pocket leading to differences in the reconstitution with retinal as for the T90V mutant of bR (*20*), e.g., the generation of other isomers instead of the all-*trans* and 13-*cis* forms. These byproducts are generated under photostationary conditions, too. Replacing the sulfhydryl group with the more electronegative hydroxyl group in C128T shifts the peak maximum by a few nanometers to the red, similar to that of the T90C mutant in bR that is blue-shifted by 10 nm (*37*) . While different factors, steric or electrostatic, can account for the observations, they nevertheless argue for the intimate location of C128 with respect to the retinal as predicted from the sequence alignment (Figure 1).

The spectral changes and especially the biphasic decay of P390 and P520 cannot be explained in a simple linear photocycle but must be a consequence of either a heterogeneous ground state with two photocycles, a branching reaction within a photocycle, or a combination of both. Both scenarios have been discussed before in describing photostationary current measurements of ChR1 (*38*) and ChR2 (*39*) with a four-state model as the minimal one. Also, other rhodopsins show complex photocycles for different reasons that could also contribute in the case of ChR2. In the chloride pump halorhodopsin, the Schiff base undergoes a slow fractional deprotonation in a branching reaction leading to a long-living M-like state (*40*, *41*). This phenomenon can also be observed in bR under hyperpolarizing conditions (*42*). The photochromicity of the *Anabaena* sensory rhodopsin relies on the light-induced interconversion between two isomeric ground states binding either all-*trans*-retinal or 13-*cis*-retinal (*43*). The photocycles are different with respect to the presence of a deprotonated Schiff base only occurring in the all-*trans* form (*44*). Conformers of the SRI−transducer complex have been described with different connectivities to the half-channels between the retinal and the aqueous phases (*45*). As a last example, microbial rhodopsins have pH-dependent ground states depending on the protonation of the counterion of the Schiff base.

Here, we adopt a branched photocycle model for the slow mutants (Figure 9). However, we cannot fully rule out the presence of two ground states leading to two different photocycles for the same reasons as mentioned above for other rhodopsins. Especially the ground-state spectra indicate slight

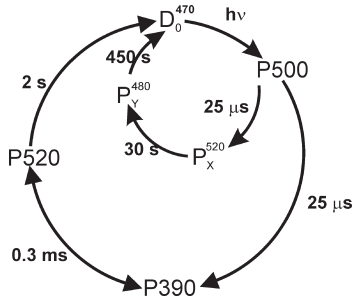

FIGURE 9: Branching model for the photocycle of C128T (for details, see the text). For consistency with the wild-type data, the spectral intermediates are denoted in the same manner, although they are spectrally shifted, leading to different peak values.

changes depending on the proton concentration (Figure 4). Nevertheless, the transition between putative forms is observed between pH 7 and 5; photointermediates P390 and P520 are already present at pH 7.4, and the changes are not dependent on mutating residue C128. The measurements on the photostationary state (Figure 5b) further support the branching model. At all pH values, the ratio of P390 and P520 correlates with their relaxation times from the single-turnover data, leading to a higher level of accumulation of P520. In contrast, the amplitude ratio changes with pH under single-turnover conditions. To understand the independence of the photostationary state from external pH, we assume that all ChR2 molecules enter the photocycle along the same pathway. The splitting takes place from an intermediate in a pH-dependent manner. The fraction of branching molecules will be determined by the protonation state of the unidentified group whose influence we detected in the single-turnover measurements and the ground-state spectra. Continuous cycling of the ChR2 molecules will eventually lead to a comparable photostationary state at different pH values, although the protonation concentration affects the molecule and its photocycle. A comparable scenario has been described for halorhodopsin (*40*, *41*). However, one should note that all the observed effects can also be explained by two intervening photocycles.

The branching model in Figure 9 accounts for our observations: (1) subsequent relaxation of two spectral intermediates, P390 and P520, that are not in a fast equilibrium (τ_3 and τ_4 in Figure 3c), (2) a pH-dependent shift of the amplitudes of P390 and P520, occurring on a fast time scale (τ_2 in Figure 3d and Figure 4c,d), and (3) photoreactions of P390 and P520, leading to an accelerated closing of the open channel (Figure 6 c; see also below). We introduced the branching reaction at the early photointermediate P500 resembling the K state of bR. Here, the retinal has isomerized to the 13-*cis* conformation as determined by FT-IR measurements (*15*, *16*). Accompanying signals in the amide I region point to large structural changes that are already observed in this stage of the photocycle. These conformational changes are sensed by the D156 residue and influence its hydrogen bonding or protonation pattern during the onset of the photocycle (*16*). In bR, similar changes by the corresponding residue D115 have been observed in FT-IR measurements (*46*). However, the structural perturbation is much smaller, and the hydrogen bond is strengthened in the K state compared to the observed upshift for D156 in ChR2. Therefore, we find in the early time region that the isomerization of the retinal shifts the opsin's conformation toward a state that has partly evolved the open pore's structure. The state of the hydrogen bond between

D156 and C128 is already affected by the different environment (*16*). It is plausible that mutating these residues will affect the photocycle in its early stage. The fraction of molecules in the branched photocycle is dependent on the type of mutation and the pH as shown in Figures 3 and 4. The C128A mutant favors the formation of the deprotonated Schiff base, while the C128T mutant splits into both photointermediates P390 and $P^{520}{}_X$ to approximately the same extent. The P390 intermediate is preferred at high pH, while the rate of its formation seems not to be affected by the proton concentration. Therefore, mutating residue C128 influences the deprotonation probability of the Schiff base on the one hand, reflected in the branching reaction, and hinders the reprotonation on the other hand, leading to the long lifetimes of photointermediate P390. Several explanations can account for this effect, i.e., a decrease in the Schiff base's pK_a, an increase in the proton donor or acceptor pK_a, or a hindered accessibility for the reprotonation pathway. Interestingly, electrostatic calculations of a bR model suggest a connectivity between the cytoplasmic side and the proton acceptor D85 via D115 (*47*, *48*), the residue corresponding to D156 in ChR2. The protonation states of both residues are dependent on each other: Deprotonating D115 at high cytoplasmic pH produces a futile pump cycle due to the protonated acceptor D85. In the case of ChR2, we can speculate that D156 exerts its effect on E123, the homologous residue of D85. However, the protonation state of this residue remains to be elucidated in response to a changing pH.

The biphasic relaxation results from the decay of $P^{520}{}_X$ and the P390−P520 equilibration. Eventually, the ground state is restored from the $P^{480}{}_Y$ intermediate that exists for minutes. In the wild type, a similar process was observed, albeit taking place in tens of seconds and from a red-shifted intermediate (*14*, *15*). The recovery of the ground state is associated with large structural reorganizations accompanied by hydrogen bonding changes for E90 and D156, whereas the retinal isomer composition of the so-called light-adapted state P480 has already equilibrated into the ground states' ratio of all-*trans*- and 13-*cis*-retinal as inferred from vibrational spectroscopy (*15*, *16*, *49*). As for the wild type, we assume a second light reaction starting from $P^{480}{}_Y$ because all molecules would be trapped in this state under continuous illumination otherwise. However, the nature of the second light reaction remains obscure so far either for the wild type or for the slow mutants.

Channel Gating and Photoreactions of the Intermediates. The models are further constrained by the electrophysiological data. Previously, we assigned the opening of the channel along with the rise of the P520 intermediate as interconversion from P390 that occurred in two phases with time constants of ~150 μs and 1 ms. With the modification and improvement of our sample preparation, the kinetics are better described with a transition of P390 to P520 in 1.5 ms (see Table 1). However, one should mention that both the buildup of P390 and the interconversion of P390 to P520 are multiphasic with an early and late microsecond process. Nevertheless, we describe the rise of P390 with a single time constant, although two are needed in some cases.

The channel concurrently closes with the relaxation of the P520 intermediate. So far, the results are consistent with the ones from ref *15*. However, we are left with the finding that the wild-type channel opens in a process (~200 μs at −20 mV and pH 7.4) that is not clearly reflected in a single process or species at the chromophore site. Both intermediates, P390 and P520, are present at least at the current onset.

For the C128A and D156A mutants, the opening of the channel is accompanied by the rise of the P520 intermediate. In the case of the C128T mutant, the electrical process is not clearly accompanied in a parallel one at the chromophore site where the opening proceeds in the early millisecond time domain with no spectral counterpart. Furthermore, the opening of the channel is retarded in the mutants by 1 order of magnitude, although the fast spectral changes (buildup of P390 and P520) are comparable. Therefore, we conclude the following. First, the channel gating is strongly influenced by conformational changes that are modulated by the mutation of C128 or D156. These changes not only are much more pronounced in ChR2 as seen in the FT-IR measurements (*15*, *16*) but also may play a more dominant role than in the photocycle of bR. Second, there is a decoupling of the kinetic processes observed at the chromophore and at the structural parts controlling the functional state of the pore. A decoupling between the transitions at the chromophore site and the pore structure is more pronounced than in the wild type. While the formation of the P390 intermediate takes place on a similar time scale as in the wild type, the opening process is retarded by 1 order of magnitude. This is not surprising for a channel in which ion permeation is decoupled from the retinal conformation and chemistry in contrast to the retinal ion pumps. The conversion of a light reaction to a conformational change at the pore is triggered either by retinal isomerization (K intermediate), i.e., a mechanical wave, by the deprotonation of the Schiff base (P390), or by the reprotonation of the Schiff base (P520), i.e., a chemical transduction. Therefore, the questions of the extent to which the P390 intermediate reflects a conducting state of the channel and which of the processes triggers the channel opening arise.

The oocyte measurements established a connection between the P390 intermediate and the open state due to the quenching effect of the violet light (400 nm). Furthermore, the relaxation time constant of the P390 decay and that for channel closing are in close agreement, suggesting that the P390 species represents the open state in the C128X mutant. On the other side, we see a green light effect as result of the photoreaction of the P520 intermediate, too, that is similar to the wild type behavior. We hypothesize that P390 is in a proton-dependent equilibrium with the subsequent state, P520. The formation of P390 is not affected by pH changes, only its decay that determines the equilibrium between these two states. The equilibrium is reflected in the changes going from P2 to P3 in the global fit analysis (Figure 3d), and it is established fast compared to its decay ($<$1 ms vs 2 s for the C128T mutant). In this simple scheme, both quenching photoreactions can be rationalized by accelerating the transition back to the ground state compared to the dark or thermal reaction. For the closing reaction, we see a fair agreement between the conductance data and the decay of the P390 and P520 intermediates. As a consequence, the second or branched photocycle leading to the long-lasting $P^{520}{}_X$ intermediate would be a nonproductive one which would raise the question about the nature and differences of the P520 intermediates in both cycles. The closing of the channel is slowed at higher proton concentrations at the cytoplasmic side in the wild type (*2*). Comparable data for the mutants from inside-out patches are not available. At least in the spectroscopic data, no strong dependence is observed in the C128T mutant for the P390−P520 decay. Therefore, we may

conclude that the sequence of events, protonation reactions and closing of the channel, is reversed in the slow mutants.

Summing up the comparison between the spectroscopic and the current measurements, we find three points remain enigmatic. (1) The identification of the branching reaction is so far a result of kinetic analysis, leaving open alternative kinetic models. The reaction itself could not assigned definitively due to the limited time resolution, and the signal-to-noise ratio of the measurements in the C128A mutant adds a higher degree of uncertainty for the early events. (2) We have two explanations for the involvement of P390 in the open state. In the first one, P390 represents a conducting species that is shut off by violet light. In the other one, the violet light effect is explained by the equilibrium between the nonconducting P390 and the conducting P520, so that depopulating P390 affects the concentration of P520, too, leading to a smaller current amplitude. (3) The occurrence of two spectrally similar P520 species with different functional roles (open in P390 and P520, closed in P^{520}_X) is based on the discrepancy in the relaxation times of channel closing and the decay of P520 in the C128T mutant. However, we cannot fully rule out an influence of the different conditions between the current and spectrocopic measurements, especially the different environment in a cellular and detergent-solubilized state. Such an influence has been observed before in the photocycle kinetics of other rhodopsins (*50*, *51*). To finally sort out the role of the two photointermediates in the open state, more experiments have to be conducted with the help of suitable mutants and the right experimental conditions.

We observe the same phenotype independent of the presence or absence of a hydrogen bonding or protonation partner at either position 128, e.g., C128A mutant, or position 156, e.g., D156A mutant. Therefore, it is not the involvement of these residues in the protonation reactions. The peculiarity is the interhelical hydrogen bond between helices 3 and 4. We think that the structural perturbation is caused by the tuning of the retinal pocket and its interaction with residue 128. For a fast closing of the channel, the interaction of helices 3 and 4 is pertinent in the closed state. The reason might be found in a direct involvement in the pore structure or the fixation of the retinal pocket via the interaction of the methyl group of C13 with C128. As we see, subtle differences at this position could lead to the loss of the steering component upon retinal isomerization due to the softening of the binding pocket. The influence on the photocycle and the channel state is the loss of a structurally guided component that controls the ordered sequence of events in ChR2.

ACKNOWLEDGMENT

We thank Anja Becker, Verena Pintschovius, and Heike Biehl for excellent technical assistance.

REFERENCES

1. Nagel, G., Ollig, D., Fuhrmann, M., Kateriya, S., Musti, A. M., Bamberg, E., and Hegemann, P. (2002) Channelrhodopsin-1: A Light-Gated Proton Channel in Green Algae. *Science 296*, 2395–2398.
2. Nagel, G., Szellas, T., Huhn, W., Kateriya, S., Adeishvili, N., Berthold, P., Ollig, D., Hegemann, P., and Bamberg, E. (2003) Channelrhodopsin-2, a directly light-gated cation-selective membrane channel. *Proc. Natl. Acad. Sci. U.S.A. 100*, 13940–13945.
3. Hegemann, P. (2008) Algal Sensory Photoreceptors. *Annu. Rev. Plant Biol. 59*, 167–189.
4. Berthold, P., Tsunoda, S. P., Ernst, O. P., Mages, W., Gradmann, D., and Hegemann, P. (2008) Channelrhodopsin-1 Initiates Phototaxis and Photophobic Responses in Chlamydomonas by Immediate Light-Induced Depolarization. *Plant Cell 20*, 1665–1677.
5. Boyden, E. S., Zhang, F., Bamberg, E., Nagel, G., and Deisseroth, K. (2005) Millisecond-timescale, genetically targeted optical control of neural activity. *Nat. Neurosci. 8*, 1263–1268.
6. Li, X., Gutierrez, D. V., Hanson, M. G., Han, J., Mark, M. D., Chiel, H., Hegemann, P., Landmesser, L. T., and Herlitze, S. (2005) Fast noninvasive activation and inhibition of neural and network activity by vertebrate rhodopsin and green algae channelrhodopsin. *Proc. Natl. Acad. Sci. U.S.A. 102*, 17816–17821.
7. Zhang, F., Wang, L.-P., Brauner, M., Liewald, J. F., Kay, K., Watzke, N., Wood, P. G., Bamberg, E., Nagel, G., Gottschalk, A., and Deisseroth, K. (2007) Multimodal fast optical interrogation of neural circuitry. *Nature 446*, 633–639.
8. Nagel, G., Brauner, M., Liewald, J. F., Adeishvili, N., Bamberg, E., and Gottschalk, A. (2005) Light Activation of Channelrhodopsin-2 in Excitable Cells of *Caenorhabditis elegans* Triggers Rapid Behavioral Responses. *Curr. Biol. 15*, 2279–2284.
9. Bi, A., Cui, J., Ma, Y.-P., Olshevskaya, E., Pu, M., Dizhoor, A. M., and Pan, Z.-H. (2006) Ectopic Expression of a Microbial-Type Rhodopsin Restores Visual Responses in Mice with Photoreceptor Degeneration. *Neuron 50*, 23–33.
10. Schroll, C., Riemensperger, T., Bucher, D., Ehmer, J., Völler, T., Erbguth, K., Gerber, B., Hendel, T., Nagel, G., Buchner, E., and Fiala, A. (2006) Light-Induced Activation of Distinct Modulatory Neurons Triggers Appetitive or Aversive Learning in *Drosophila* Larvae. *Curr. Biol. 16*, 1741–1747.
11. Douglass, A. D., Kraves, S., Deisseroth, K., Schier, A. F., and Engert, F. (2008) Escape Behavior Elicited by Single, Channelrhodopsin-2-Evoked Spikes in Zebrafish Somatosensory Neurons. *Curr. Biol. 18*, 1133–1137.
12. Han, X., Qian, X., Bernstein, J. G., Zhou, H.-h., Franzesi, G. T., Stern, P., Bronson, R. T., Graybiel, A. M., Desimone, R., and Boyden, E. S. (2009) Millisecond-Timescale Optical Control of Neural Dynamics in the Nonhuman Primate Brain. *Neuron 62*, 191–198.
13. Lanyi, J. K. (2004) Bacteriorhodopsin. *Annu. Rev. Physiol. 66*, 665–688.
14. Bamann, C., Kirsch, T., Nagel, G., and Bamberg, E. (2008) Spectral Characteristics of the Photocycle of Channelrhodopsin-2 and Its Implication for Channel Function. *J. Mol. Biol. 375*, 686–694.
15. Ritter, E., Stehfest, K., Berndt, A., Hegemann, P., and Bartl, F. J. (2008) Monitoring Light-induced Structural Changes of Channelrhodopsin-2 by UV-visible and Fourier Transform Infrared Spectroscopy. *J. Biol. Chem. 283*, 35033–35041.
16. Radu, I., Bamann, C., Nack, M., Nagel, G., Bamberg, E., and Heberle, J. (2009) Conformational Changes of Channelrhodopsin-2. *J. Am. Chem. Soc. 131*, 7313–7319.
17. Berndt, A., Yizhar, O., Gunaydin, L. A., Hegemann, P., and Deisseroth, K. (2009) Bi-stable neural state switches. *Nat. Neurosci. 12*, 229–234.
18. Ihara, K., Umemura, T., Katagiri, I., Kitajima-Ihara, T., Sugiyama, Y., Kimura, Y., and Mukohata, Y. (1999) Evolution of the archaeal rhodopsins: evolution rate changes by gene duplication and functional differentiation. *J. Mol. Biol. 285*, 163–174.
19. Luecke, H., Schobert, B., Richter, H.-T., Cartailler, J.-P., and Lanyi, J. K. (1999) Structure of bacteriorhodopsin at 1.55 Å resolution. *J. Mol. Biol. 291*, 899–911.
20. Marti, T., Otto, H., Mogi, T., Rosselet, S. J., Heyn, M. P., and Khorana, H. G. (1991) Bacteriorhodopsin mutants containing single substitutions of serine or threonine residues are all active in proton translocation. *J. Biol. Chem. 266*, 6919–6927.
21. Peralvarez-Marin, A., Marquez, M., Bourdelande, J.-L., Querol, E., and Padros, E. (2004) Thr-90 Plays a Vital Role in the Structure and Function of Bacteriorhodopsin. *J. Biol. Chem. 279*, 16403–16409.
22. Andre, N., Cherouati, N., Prual, C., Steffan, T., Zeder-Lutz, G., Magnin, T., Pattus, F., Michel, H., Wagner, R., and Reinhart, C. (2006) Enhancing functional production of G protein-coupled receptors in *Pichia pastoris* to levels required for structural studies via a single expression screen. *Protein Sci. 15*, 1115–1126.
23. Ernst, O. P., Murcia, P. A. S., Daldrop, P., Tsunoda, S. P., Kateriya, S., and Hegemann, P. (2008) Photoactivation of Channelrhodopsin. *J. Biol. Chem. 283*, 1637–1643.
24. Scharf, B., Hess, B., and Engelhard, M. (1992) Chromophore of sensory rhodopsin II from *Halobacterium halobium*. *Biochemistry 31*, 12486–12492.
25. Takahashi, T., Yan, B., Mazur, P., Derguini, F., Nakanishi, K., and Spudich, J. L. (1990) Color regulation in the archaebacterial phototaxis receptor phoborhodopsin (sensory rhodopsin II). *Biochemistry 29*, 8467–8474.

26. Tsunoda, S. P., and Hegemann, P. (2009) Glu 87 of Channelrhodopsin-1 Causes pH-dependent Color Tuning and Fast Photocurrent Inactivation. *Photochem. Photobiol. 85*, 564–569.
27. Chizhov, I., Schmies, G., Seidel, R., Sydor, J. R., Luttenberg, B., and Engelhard, M. (1998) The Photophobic Receptor from *Natronobacterium pharaonis*: Temperature and pH Dependencies of the Photocycle of Sensory Rhodopsin II. *Biophys. J. 75*, 999–1009.
28. Friedrich, T., Geibel, S., Kalmbach, R., Chizhov, I., Ataka, K., Heberle, J., Engelhard, M., and Bamberg, E. (2002) Proteorhodopsin is a Light-driven Proton Pump with Variable Vectoriality. *J. Mol. Biol. 321*, 821–838.
29. Zhu, J., Spudich, E. N., Alam, M., and Spudich, J. L. (1997) Effects of Substitutions D73E, D73N, D103N and V106M on Signaling and pH Titration of Sensory Rhodopsin II. *Photochem. Photobiol. 66*, 788–791.
30. Subramaniam, S., Marti, T., and Khorana, H. G. (1990) Protonation state of Asp (Glu)-85 regulates the purple-to-blue transition in bacteriorhodopsin mutants Arg-82 → Ala and Asp-85 → Glu: The blue form is inactive in proton translocation. *Proc. Natl. Acad. Sci. U. S.A. 87*, 1013–1017.
31. Karvaly, B., and Dancsházy, Z. (1977) Bacteriorhodopsin: A molecular photoelectric regulator quenching of photovoltaic effect of bimolecular lipid membranes containing bacteriorhodopsin by blue light. *FEBS Lett. 76*, 36–40.
32. Butt, H. J., Fendler, K., Bamberg, E., Tittor, J., and Oesterhelt, D. (1989) Aspartic acids 96 and 85 play a central role in the function of bacteriorhodopsin as a proton pump. *EMBO J. 8*, 1657–1663.
33. Ormos, P., Dancshazy, Z., and Keszthelyi, L. (1980) Electric response of a back photoreaction in the bacteriorhodopsin photocycle. *Biophys. J. 31*, 207–213.
34. Feldbauer, K., Zimmermann, D., Pintschovius, V., Spitz, J., Bamann, C., and Bamberg, E. (2009) Channelrhodopsin-2 is a leaky proton pump. *Proc. Natl. Acad. Sci. U.S.A. 106*, 12317–12322.
35. Lin, J. Y., Lin, M. Z., Steinbach, P., and Tsien, R. Y. (2009) Characterization of Engineered Channelrhodopsin Variants with Improved Properties and Kinetics. *Biophys. J. 96*, 1803–1814.
36. Banghart, M. R., Volgraf, M., and Trauner, D. (2006) Engineering Light-Gated Ion Channels. *Biochemistry 45*, 15129–15141.
37. Flitsch, S. L., and Khorana, H. G. (1989) Structural studies on transmembrane proteins. 1. Model study using bacteriorhodopsin mutants containing single cysteine residues. *Biochemistry 28*, 7800–7805.
38. Hegemann, P., Ehlenbeck, S., and Gradmann, D. (2005) Multiple Photocycles of Channelrhodopsin. *Biophys. J. 89*, 3911–3918.
39. Nikolic, K., Grossman, N., Grubb, M. S., Burrone, J., Toumazou, C., and Degenaar, P. (2009) Photocycles of Channelrhodopsin-2. *Photochem. Photobiol. 85*, 400–411.
40. Bamberg, E., Tittor, J., and Oesterhelt, D. (1993) Light-Driven Proton or Chloride Pumping by Halorhodopsin. *Proc. Natl. Acad. Sci. U.S.A. 90*, 639–643.
41. Hegemann, P., Oesterhelt, D., and Steiner, M. (1985) The photocycle of the chloride pump halorhodopsin. I: Azide-catalyzed deprotonation of the chromophore is a side reaction of photocycle intermediates inactivating the pump. *EMBO J. 4*, 2347–2350.
42. Geibel, S., Friedrich, T., Ormos, P., Wood, P. G., Nagel, G., and Bamberg, E. (2001) The Voltage-Dependent Proton Pumping in Bacteriorhodopsin Is Characterized by Optoelectric Behavior. *Biophys. J. 81*, 2059–2068.
43. Vogeley, L., Sineshchekov, O. A., Trivedi, V. D., Sasaki, J., Spudich, J. L., and Luecke, H. (2004) *Anabaena* Sensory Rhodopsin: A Photochromic Color Sensor at 2.0 Å. *Science 306*, 1390–1393.
44. Shi, L., Yoon, S. R., Bezerra, J. A. G., Jung, K.-H., and Brown, L. S. (2006) Cytoplasmic Shuttling of Protons in *Anabaena* Sensory Rhodopsin: Implications for Signaling Mechanism. *J. Mol. Biol. 358*, 686–700.
45. Sineshchekov, O. A., Sasaki, J., Phillips, B. J., and Spudich, J. L. (2008) A Schiff base connectivity switch in sensory rhodopsin signaling. *Proc. Natl. Acad. Sci. U.S.A. 105*, 16159–16164.
46. Braiman, M. S., Mogi, T., Marti, T., Stern, L. J., Khorana, H. G., and Rothschild, K. J. (1988) Vibrational spectroscopy of bacteriorhodopsin mutants: Light-driven proton transport involves protonation changes of aspartic acid residues 85, 96, and 212. *Biochemistry 27*, 8516–8520.
47. Bombarda, E., Becker, T., and Ullmann, G. M. (2006) Influence of the Membrane Potential on the Protonation of Bacteriorhodopsin: Insights from Electrostatic Calculations into the Regulation of Proton Pumping. *J. Am. Chem. Soc. 128*, 12129–12139.
48. Calimet, N., and Matthias Ullmann, G. (2004) The Influence of a Transmembrane pH Gradient on Protonation Probabilities of Bacteriorhodopsin: The Structural Basis of the Back-Pressure Effect. *J. Mol. Biol. 339*, 571–589.
49. Nack, M., Radu, I., Bamann, C., Bamberg, E., and Heberle, J. (2009) The retinal structure of channelrhodopsin-2 assessed by resonance Raman spectroscopy. *FEBS Lett. 583*, 3676–3680.
50. Duschl, A., McCloskey, M. A., and Lanyi, J. K. (1988) Functional reconstitution of halorhodopsin. Properties of halorhodopsin-containing proteoliposomes. *J. Biol. Chem. 263*, 17016–17022.
51. Milder, S. J., Thorgeirsson, T. E., Miercke, L. J. W., Stroud, R. M., and Kliger, D. S. (1991) Effects of detergent environments on the photocycle of purified monomeric bacteriorhodopsin. *Biochemistry 30*, 1751–1761.
52. Kiefer, F., Arnold, K., Kunzli, M., Bordoli, L., and Schwede, T. (2009) The SWISS-MODEL Repository and associated resources. *Nucleic Acids Res. 37*, D387–D392.
53. Humphrey, W., Dalke, A., and Schulten, K. (1996) VMD: Visual Molecular Dynamics. *J. Mol. Graphics 14*, 33–38.